



Article

Non-Covalent Interactions Involving Alkaline-Earth Atoms and Lewis Bases B: An ab Initio Investigation of Beryllium and Magnesium Bonds, $B\cdots MR_2$ ($M = \text{Be or Mg}$, and $R = \text{H, F or CH}_3$)

Ibon Alkorta ^{1,*} and Anthony C. Legon ^{2,*} ¹ Instituto de Química Médica (IQM-CSIC), Juan de la Cierva, 3, E-28006 Madrid, Spain² School of Chemistry, University of Bristol, Cantock's Close, Bristol BS8 1TS, UK* Correspondence: ibon@iqm.csic.es (I.A.); a.c.legon@bristol.ac.uk (A.C.L.);
Tel.: +44-117-331-7708 (A.C.L.); +34-912587675 (I.A.)

Received: 30 January 2019; Accepted: 26 February 2019; Published: 5 March 2019



Abstract: Geometries, equilibrium dissociation energies (D_e), intermolecular stretching, and quadratic force constants (k_σ) determined by ab initio calculations conducted at the CCSD(T)/aug-cc-pVTZ level of theory, with D_e obtained by using the complete basis set (CBS) extrapolation [CCSD(T)/CBS energy], are presented for the $B\cdots BeR_2$ and $B\cdots MgR_2$ complexes, where B is one of the following Lewis bases: CO, H₂S, PH₃, HCN, H₂O or NH₃, and R is H, F or CH₃. The BeR₂ and MgR₂ precursor molecules were shown to be linear and non-dipolar. The non-covalent intermolecular bond in the $B\cdots BeR_2$ complexes is shown to result from the interaction of the electrophilic band around the Be atom of BeR₂ (as indicated by the molecular electrostatic potential surface) with non-bonding electron pairs of the base, B, and may be described as a beryllium bond by analogy with complexes such as $B\cdots CO_2$, which contain a tetrel bond. The conclusions for the $B\cdots MgR_2$ series are similar and a magnesium bond can be correspondingly invoked. The geometries established for $B\cdots BeR_2$ and $B\cdots MgR_2$ can be rationalized by a simple rule previously enunciated for tetrel-bonded complexes of the type $B\cdots CO_2$. It is also shown that the dissociation energy, D_e , is directly proportional to the force constant, k_σ , in each $B\cdots MR_2$ series, but with a constant of proportionality different from that established for many hydrogen-bonded $B\cdots HX$ complexes and halogen-bonded $B\cdots XY$ complexes. The values of the electrophilicity, E_A , determined from the D_e for $B\cdots BeR_2$ complexes for the individual Lewis acids, A, reveal the order $A = BeF_2 > BeH_2 > Be(CH_3)_2$ —a result that is consistent with the $-I$ and $+I$ effects of F and CH₃ relative to H. The conclusions for the MgR₂ series are similar but, for a given R, they have smaller electrophilicities than those of the BeR₂ series. A definition of alkaline-earth non-covalent bonds is presented.

Keywords: magnesium bonds; beryllium bonds; ab initio calculations; binding strength; electrophilicity and nucleophilicity

1. Introduction

The non-covalent interactions of closed-shell molecules represent an important subject in many areas of chemistry and biology. The central position of the hydrogen bond in these disciplines is well known. Since the 1950s, there has been a rapid growth of interest in other non-covalent interactions. The halogen bond was first named and identified experimentally in the solid state in the 1950s by Hassel [1], and then in the gas phase as a weak interaction involving simple Lewis bases with di-halogen molecules in the 1990s [2]. The halogen bond was shown [2,3] to have properties similar to those of the hydrogen bond. Interest in the halogen bond has grown rapidly within chemistry, biology

and materials science in the last two decades [4,5]. The comprehensive definitions of the hydrogen bond and the halogen bond by working parties set up by IUPAC were published in 2011 [6] and 2013 [7], respectively. The definition of the halogen bond explicitly invokes the interaction of a halogen atom (acting as an electrophile) with a non-bonding or π -bonding electron pair (the nucleophilic region) of, for example, a Lewis base. Tetrel bonds, pnictogen bonds, and chalcogen bonds are non-covalent interactions that have been investigated extensively in the gas phase [8] and condensed phase [9] since the 1970s, but were only named according to the group in the periodic table from which the atom acting as the electrophile originates (Groups 14, 15 and 16, respectively) in 2013 [10], 2011 [11], and 2009 [12], respectively. The IUPAC definitions of these newer types of interactions, similar to that of the halogen bond, are imminent [13]. However, the general applicability of such definitions based on electrostatics alone has been questioned in the case of some of the more unusual types of non-covalent interactions [14–17]. Other non-covalent interactions involving atoms of other groups in the periodic table acting as the electrophilic region can be identified. A recent example is the so-called coinage-metal bond $B \cdots MX$, where B is a Lewis base and M is a Group 11 metal atom [18].

In this article, we report an investigation, by means of high-level ab initio calculations, of $B \cdots BeR_2$ and $B \cdots MgR_2$ complexes in which B is one of the six simple Lewis bases CO, H_2S , PH_3 , HCN, H_2O or NH_3 and R is H, F or CH_3 . We will show that various Lewis acid molecules, BeR_2 and MgR_2 , are linear, non-dipolar, and of geometry $R-Be-R$ and $R-Mg-R$. In each case, we also show, from the molecular electrostatic surface potentials, that there is a positive belt around the central Group 2 atom which can act as the electrophilic region when forming either a beryllium or a magnesium bond [19] to the most nucleophilic region (a non-bonding electron pair) of the Lewis base. As well as the geometry optimizations of the complexes, we also calculate two measures of the binding strength, namely, the equilibrium dissociation energy, D_e , and the intermolecular stretching force constant, traditionally referred to as k_σ [2]. The first is the energy required to remove the component molecules from the hypothetical equilibrium separation to infinite distance, while the second is a measure of the work required for a unit infinitesimal displacement from the equilibrium. It has been shown [20–22] that for a wide range of hydrogen-, halogen-, tetrel-, pnictogen- and chalcogen-bonded complexes, D_e is directly proportional to k_σ and, moreover, that it is possible to reproduce the D_e values (and, therefore, the k_σ values also) by assigning a set of electrophilicities, E_A , to the Lewis acids, A, and nucleophilicities, N_B , to the Lewis bases, B. An important aim of the present article is to discover whether this partitioning also applies to beryllium- and magnesium-bonded complexes.

Another aim of this study is to examine the effects of replacing both H atoms in $H-Be-H$ and $H-Mg-H$, firstly by F and secondly by CH_3 groups. According to the electronic theory of organic chemistry developed by Ingold [23] and in particular the inductive effect I, F removes electronic charge from the central atom relative to the hydride (the $-I$ effect), while the methyl group pushes electrons towards the central atom through the $+I$ effect. If so, the central Group 2 atom should become more electrophilic (E_A should increase relative to that of the dihydride) in $F-Be-F$ and $F-Mg-F$, but less electrophilic (decrease of E_A) in $CH_3-Be-CH_3$ and $CH_3-Mg-CH_3$. This conclusion is confirmed by the molecular electrostatic potential surfaces (MEPS) of $F-Be-F$, $H-Be-H$ and $CH_3-Be-CH_3$. These were calculated for the 0.001 e/bohr^3 electron density isosurface at the CCSD/aug-cc-pVTZ//CCSD(T)/aug-cc-pVTZ level of theory with the Gaussian-16 Program [24] and are shown in Figure 1. In each case, there is a blue belt that surrounds the central Be atoms. The deepest blue color corresponds to the most positive MEPS in each case and has a maximum value of 337, 167 and $119 \text{ kJ} \cdot \text{mol}^{-1}$ for $F-Be-F$, $H-Be-H$ and $CH_3-Be-CH_3$, respectively. Thus, the blue belt surrounding the Be atom is the most electrophilic region in each molecule and the electrophilicity is greatest when F is the ligand and smallest when CH_3 is the ligand, in agreement with the $-I$ and $+I$ inductive effects of F and CH_3 , respectively. Similar patterns are observed from the MEPSs of the Mg analogues (see Supplementary Material, Figure S1), except that for a given ligand, R, the maximum positive potential is higher for Mg than for Be, with values of 753, 321 and $280 \text{ kJ} \cdot \text{mol}^{-1}$, for $R = F$, H and CH_3 , respectively.

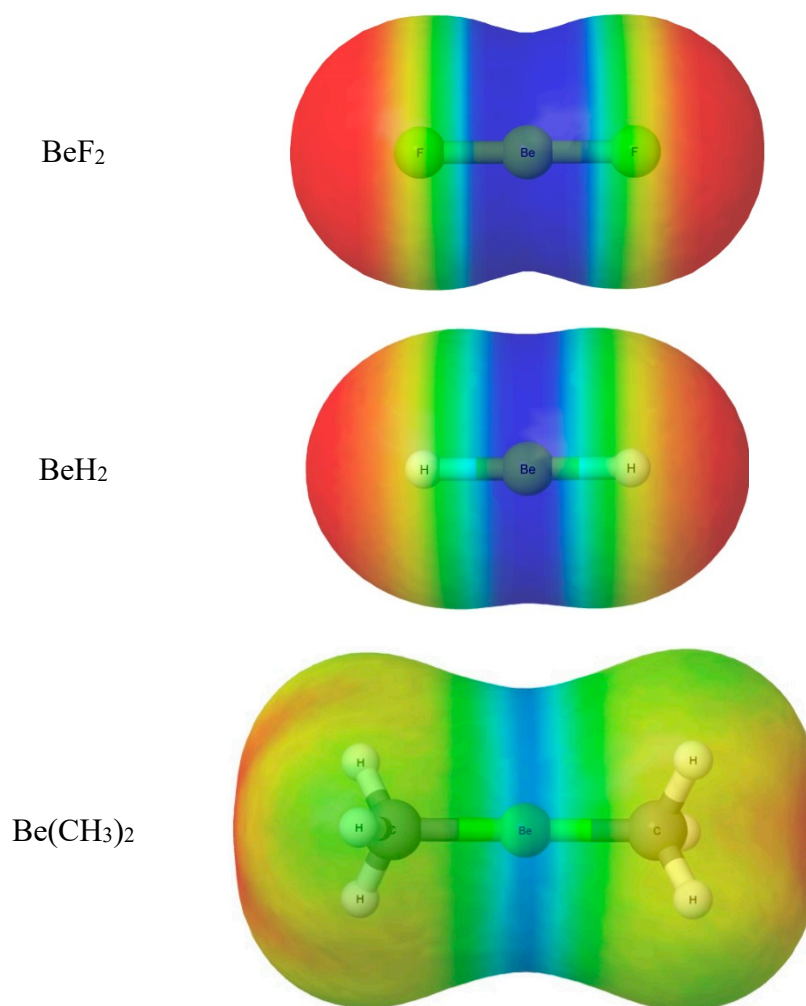


Figure 1. Molecular electrostatic potential surfaces of the linear non-polar molecules, BeF_2 , BeH_2 and $\text{Be}(\text{CH}_3)_2$ calculated at the 0.001 e/bohr³ electron density isosurface at the CCSD/ aug-cc-pVTZ // CCSD(T)/aug-cc-pVTZ level of theory. The surface has been made transparent to reveal the molecular model within. The most intense blue (and, therefore, the most electrophilic) belts centered on Be correspond to positive electrostatic potential energies of 337, 167 and 119 kJ·mol^{−1} for BeF_2 , BeH_2 and $\text{Be}(\text{CH}_3)_2$, respectively, and confirm expectations based on the inductive effects of CH_3 and F relative to H.

2. Results

2.1. Molecular Geometries

The molecular diagrams (drawn to scale) of the geometries of the three Lewis acids BeF_2 , BeH_2 and $\text{Be}(\text{CH}_3)_2$ optimized at the CCSD(T)/aug-cc-pVTZ level of theory are shown in Figure 2. The geometries belong to the point groups $D_{\infty h}$, $D_{\infty h}$ and D_{3d} , respectively, and are consistent with two singly occupied sp hybrid orbitals on the central Be atom forming bonds with F, H or C, respectively. The similarly determined geometries for the three Mg analogues are isostructural with their Be counterparts, but are not shown. They are available from the Supplementary Material, which includes the optimized cartesian coordinates of atoms for all molecules investigated here.

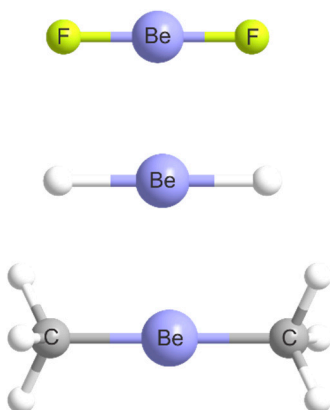


Figure 2. Geometries of BeF_2 , BeH_2 and $\text{Be}(\text{CH}_3)_2$ optimized at the CCSD(T)/aug-cc-pVTZ level of theory (to scale).

Figure 3 displays the molecular diagrams (drawn to scale) of the six $\text{B} \cdots \text{BeF}_2$ complexes in which $\text{B} = \text{CO}$, HCN , H_2O , NH_3 , H_2S or PH_3 . The molecular diagrams of the corresponding sets of six $\text{B} \cdots \text{BeH}_2$ and $\text{B} \cdots \text{Be}(\text{CH}_3)_2$ complexes are shown in Figures 4 and 5, respectively. In each case, the fragment $\text{R}_2\text{Be} \cdots \text{L}$, where L is the atom of B involved in the intermolecular bond, is Y-shaped (local symmetry C_{2v}). Thus, the angle, θ (which is defined in Figure 3), is zero in the BeR_2 monomer molecules, but increases significantly in all $\text{B} \cdots \text{BeR}_2$ complexes investigated, as indicated by the values included in Table 1. The Y shape can be explained if it is assumed that, when the Lewis base, B , approaches $\text{R}-\text{Be}-\text{R}$ and forms the complex, the hybridization at the central Be atom starts to change to sp^2 and the third (empty) sp^2 orbital receives the non-bonding electron pair of B with the result that a partial dative bond $\text{Be}-\text{L}$ is formed with the acceptor atom of B . It is clear from Table 1 that the angles $\text{R}-\text{Be}-\text{R}$ are all less than 180° in the $\text{B} \cdots \text{BeR}_2$ complexes but are greater than the ideal sp^2 angles of 120° that would occur for a fully dative bond (*i.e.*, $0^\circ < \theta < 30^\circ$). The BeCl_3^- anion [25] has three equivalent $\text{Be}-\text{Cl}$ bonds and D_{3h} symmetry, with ideal 120° angles. There are also increases δr in the distances $r(\text{R}-\text{Be})$ on formation of all $\text{B} \cdots \text{BeR}_2$ complexes considered here, as expected for the partial change from sp to sp^2 hybridization at Be . The values of δr for all $\text{B} \cdots \text{BeR}_2$ complexes investigated are included in Table 1.

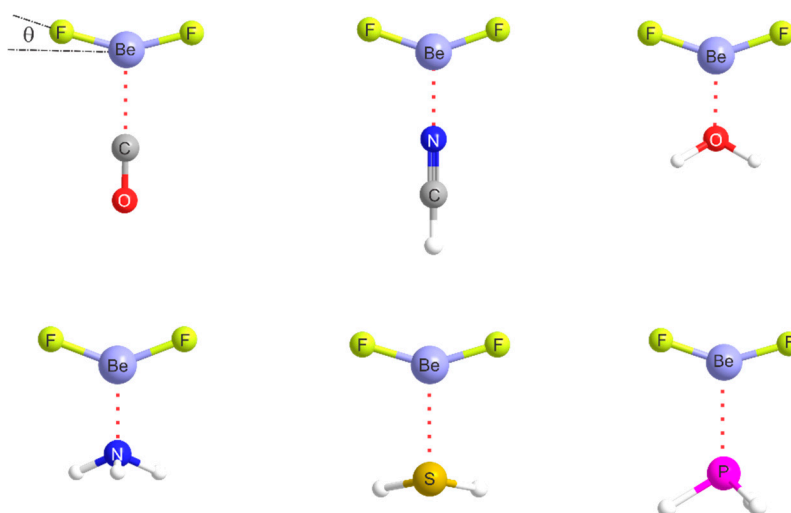


Figure 3. Geometries (drawn to scale) of six $\text{B} \cdots \text{BeF}_2$ complexes optimized at the CCSD(T)/aug-cc-pVTZ level of theory, where $\text{B} = \text{CO}$, HCN , H_2O , NH_3 , H_2S and PH_3 .

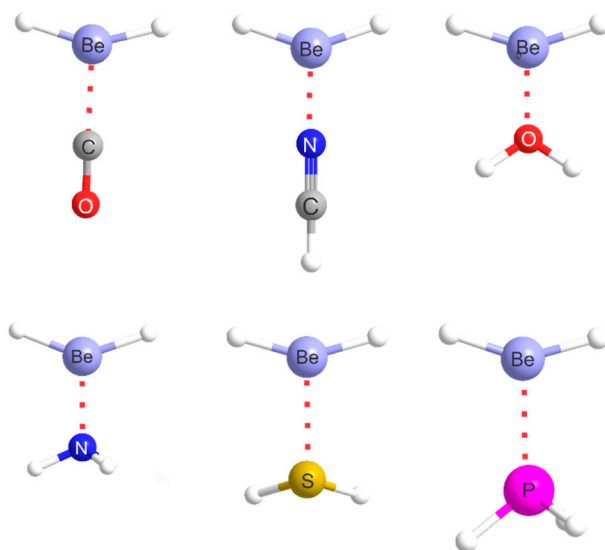


Figure 4. Geometries (drawn to scale) of six $B \cdots BeH_2$ complexes optimized at the CCSD(T)/aug-cc-pVTZ level of theory, where $B = CO, HCN, H_2O, NH_3, H_2S$ and PH_3 .

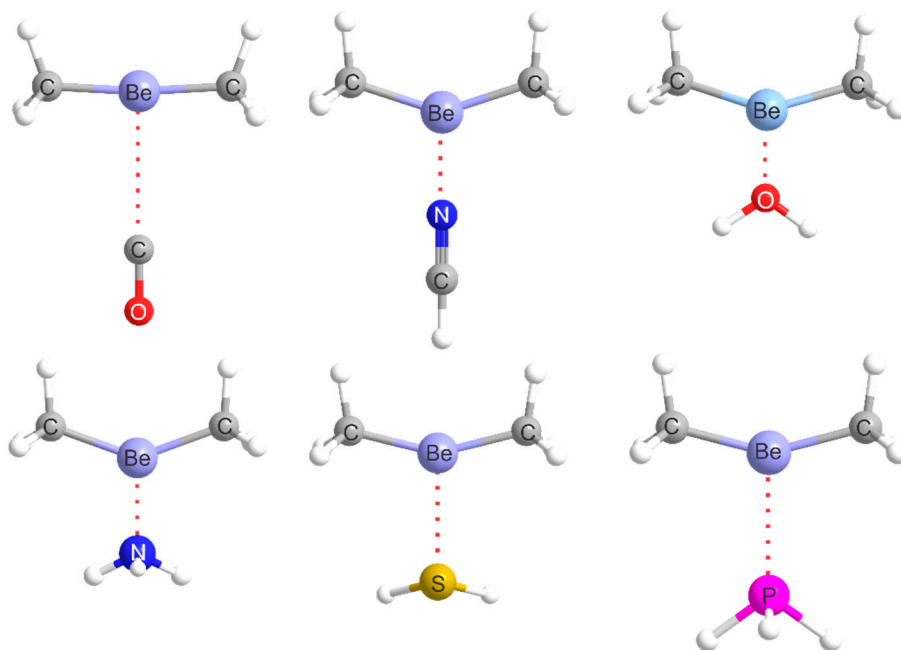


Figure 5. Geometries (drawn to scale) of six $B \cdots Be(CH_3)_2$ complexes optimized at the CCSD(T)/aug-cc-pVTZ level of theory, where $B = CO, HCN, H_2O, NH_3, H_2S$ and PH_3 .

The observations about the angle θ and the increase δr in the distances $r(R-Mg)$ also apply to the formation of the $B \cdots MgR_2$ complexes from the various MgR_2 molecules. Table 2 includes these quantities for the 18 complexes that result from the interaction of the three MgR_2 molecules ($R = F, H$ or CH_3) with the set of six Lewis bases, $B = CO, HCN, H_2O, NH_3, H_2S$ or PH_3 . The full geometries of these complexes are available in the form of the cartesian coordinates in the Supplementary Material. We note from Tables 1 and 2 that the distance $r(Mg \cdots L)$ is correlated with the strength of the interaction in the Mg series, in the sense that shorter distances are associated with larger D_e values; the correlation is less clear in the Be series.

Table 1. Some ab initio calculated properties of the B...BeR₂ complexes (R = F, H or CH₃) for six different Lewis bases B ^a.

Complex	Lewis Base B	$D_e/\text{kJ}\cdot\text{mol}^{-1}$	$k_\sigma/\text{N}\cdot\text{m}^{-1}$	$r(\text{Be}\cdots\text{A})/\text{\AA}$ ^b	Angle $\theta/^\circ$ ^c	$\delta r(\text{Be}-\text{R})/\text{\AA}$ ^d
B...BeF ₂	CO	26.72	36.33	2.040	15.0	0.024
	NCH	66.98	87.59	1.818	19.2	0.035
	H ₂ O	95.94	121.89	1.697	18.7	0.040
	NH ₃	121.73	133.19	1.777	21.1	0.045
	H ₂ S	43.57	44.59	2.289	16.9	0.029
	PH ₃	41.59	45.87	2.337	17.7	0.035
B...BeH ₂	CO	21.29	44.61	1.942	16.3	0.019
	NCH	53.67	85.38	1.790	19.1	0.026
	H ₂ O	80.94	110.93	1.688	18.0	0.030
	NH ₃	102.10	123.11	1.783	20.5	0.035
	H ₂ S	34.58	37.91	2.270	16.0	0.021
	PH ₃	34.08	42.86	2.305	17.0	0.023
B...Be(CH ₃) ₂	CO	5.28	2.00	2.922	3.2	0.004
	NCH	32.75	57.73	1.844	18.1	0.035
	H ₂ O	57.82	82.21	1.720	18.7	0.040
	NH ₃	77.89	104.24	1.809	20.0	0.046
	H ₂ S	16.97	14.07	2.425	14.1	0.025
	PH ₃	14.19	15.02	2.456	14.8	0.027

^a Calculations were performed at the CCSD(T)/aug-ccpVTZ level. D_e was obtained from a complete basis set (CBS) extrapolation. See Section 3 for details. ^b $r(\text{Be}\cdots\text{A})$ is the distance between the Be atom and the nearest atom, L, of the Lewis base B. ^c The angle, θ , is the angular displacement of each group, R, in the complex from the straight line, R–Be–R defined in the free molecule (see Figure 3). ^d $\delta r(\text{Be}-\text{R})$ is the increase in the Be–R bond length (R = F, H or CH₃) when B...BeR₂ is formed from B and BeR₂.

Table 2. Some ab initio calculated properties of the B...MgR₂ complexes (R = F, H or CH₃) for six different Lewis bases B ^a.

Complex	Lewis Base B	$D_e/\text{kJ}\cdot\text{mol}^{-1}$	$k_\sigma/\text{N}\cdot\text{m}^{-1}$	$r(\text{Mg}\cdots\text{A})/\text{\AA}$ ^b	Angle $\theta/^\circ$ ^c	$\delta r(\text{Mg}-\text{R})/\text{\AA}$ ^d
B...MgF ₂	CO	36.67	39.70	2.396	8.7	0.011
	NCH	76.80	72.72	2.178	14.1	0.019
	H ₂ O	99.36	97.67	2.046	11.4	0.021
	NH ₃	114.69	90.21	2.163	14.1	0.024
	H ₂ S	56.03	44.02	2.631	10.8	0.016
	PH ₃	53.01	41.96	2.703	11.7	0.017
B...MgH ₂	CO	18.57	16.81	2.567	7.6	0.008
	NCH	49.62	45.08	2.269	13.0	0.019
	H ₂ O	70.81	68.88	2.111	11.3	0.023
	NH ₃	82.05	64.97	2.233	14.0	0.028
	H ₂ S	33.59	23.74	2.777	9.7	0.015
	PH ₃	30.33	21.81	2.854	9.9	0.015
B...Mg(CH ₃) ₂	CO	16.52	13.76	2.609	6.5	0.006
	NCH	45.33	41.10	2.285	12.2	0.015
	H ₂ O	64.50	64.03	2.124	11.1	0.019
	NH ₃	75.78	61.13	2.245	13.5	0.023
	H ₂ S	30.79	20.72	2.808	8.5	0.011
	PH ₃	27.12	18.85	2.892	8.9	0.012

^a Calculations were performed at the CCSD(T)/aug-ccpVTZ level. D_e was obtained from a complete basis set (CBS) extrapolation. See Section 3 for details. ^b $r(\text{Mg}\cdots\text{L})$ is the distance between the Mg atom and the nearest atom, L, of the Lewis base B. ^c The angle, θ , is the angular displacement of each group, R, in the complex from the straight line, R–Mg–R defined in the free molecule (see Figure 3). ^d $\delta r(\text{Mg}-\text{R})$ is the increase in the Mg–R bond length (R = F, H or CH₃) when B...MgR₂ is formed from B and MgR₂.

2.2. Relationship between D_e and k_σ

The two measures (D_e and k_σ) of the binding strength obtained through ab initio calculations for the 18 B...BeR₂ complexes discussed in Section 2.1 are given in Table 1. The corresponding quantities for the 18 B...MgR₂ are in Table 2. It should be noted, from Tables 1 and 2, that these complexes

tend to be more strongly bound according to both criteria (D_e and k_σ) than those of a wide range of hydrogen-, halogen-, tetrel-, pnictogen- and chalcogen-bonded complexes with a similar set of Lewis bases previously investigated [20–22]. Typically, for the hydrogen- and halogen-bonded complexes considered in [22], for example, $D_e \approx 20 \text{ kJ}\cdot\text{mol}^{-1}$ and $k_\sigma \approx 10 \text{ N}\cdot\text{m}^{-1}$. This larger binding strength of the $\text{B}\cdots\text{BeR}_2$ and $\text{B}\cdots\text{MgR}_2$ complexes is reflected in the significant geometrical distortions in BeR_2 and MgR_2 on complex formation noted in Section 2.1. Given the direct proportionality of D_e and k_σ established in refs. [20–22] for hydrogen- and halogen-bonded complexes, it is of interest to examine whether a similar relationship between the two quantities holds for the $\text{B}\cdots\text{BeR}_2$ and $\text{B}\cdots\text{MgR}_2$ complexes discussed here.

Figure 6 shows a plot of D_e versus k_σ for the 18 $\text{B}\cdots\text{BeR}_2$ complexes ($\text{B} = \text{CO}, \text{HCN}, \text{H}_2\text{O}, \text{NH}_3, \text{H}_2\text{S}$ or PH_3 ; $\text{R} = \text{F}, \text{H}$ or CH_3). The result of a linear regression fit to the points is also shown. The points lie on a reasonably good straight line, which passes through the origin. Two minima at the CCSD(T)/aug-cc-pVTZ level were found for $\text{OC}\cdots\text{Be}(\text{CH}_3)_2$. The first minimum occurs at a $\text{Be}\cdots\text{C}$ distance of 2.19 \AA with $D_e = 3.66 \text{ kJ}\cdot\text{mol}^{-1}$, while the second (and global) minimum is at 2.92 \AA with D_e of $5.28 \text{ kJ}\cdot\text{mol}^{-1}$. The barrier between the two minima is less than $0.01 \text{ kJ}\cdot\text{mol}^{-1}$. Figure 7 is the plot of D_e versus k_σ for the 18 $\text{B}\cdots\text{MgR}_2$ complexes. Thus, as found for a wide range of hydrogen-bonded $\text{B}\cdots\text{HX}$ complexes, halogen-bonded $\text{B}\cdots\text{XY}$ complexes and tetrel-, pnictogen- and chalcogen-bonded complexes [20,21], D_e is, in good approximation, directly proportional to k_σ for both $\text{B}\cdots\text{BeR}_2$ and $\text{B}\cdots\text{MgR}_2$ series; that is, $D_e = c' \cdot k_\sigma$, where c' is the constant of proportionality.

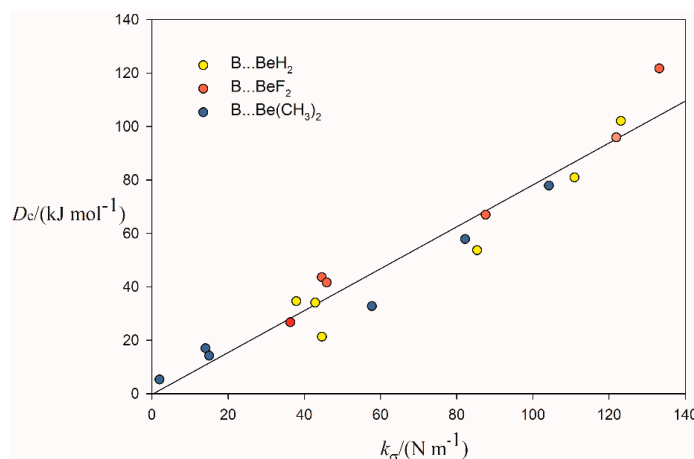


Figure 6. Variation of ab initio-calculated values of D_e with k_σ for 18 $\text{B}\cdots\text{BeR}_2$ complexes ($\text{R} = \text{F}, \text{H}$ or CH_3 ; $\text{B} = \text{CO}, \text{HCN}, \text{H}_2\text{O}, \text{NH}_3, \text{H}_2\text{S}$ or PH_3). For the linear regression, $R^2 = 0.939$.

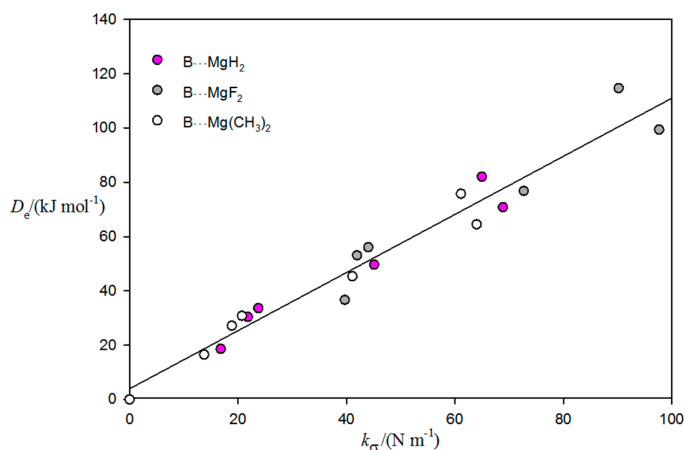


Figure 7. Variation of ab initio-calculated values of D_e with k_σ for 18 $\text{B}\cdots\text{MgR}_2$ complexes ($\text{R} = \text{F}, \text{H}$ or CH_3 ; $\text{B} = \text{CO}, \text{HCN}, \text{H}_2\text{O}, \text{NH}_3, \text{H}_2\text{S}$ or PH_3). For the linear regression, $R^2 = 0.952$.

Although a single value of $c' = 1.40(4) \times 10^3 \text{ m}^2 \cdot \text{mol}^{-1}$ was obtained by fitting all five types of complexes (hydrogen-, halogen-, tetrel-, pnictogen- and chalcogen-bonded) discussed in [20], the values of c' obtained from the linear regressions in Figures 6 and 7 for $\text{B} \cdots \text{BeR}_2$ and $\text{B} \cdots \text{MgR}_2$ are significantly smaller at $0.79(5) \times 10^3 \text{ m}^2 \cdot \text{mol}^{-1}$ and $1.07(6) \times 10^3 \text{ m}^2 \cdot \text{mol}^{-1}$, respectively. It should be noted, however, that the beryllium and magnesium bonds considered here are much stronger for a given B and the molecular distortions on formation of these bonds are greater than those for the other five types of non-covalent interactions listed. Plots of D_e versus k_σ for $\text{B} \cdots \text{BeR}_2$ and $\text{B} \cdots \text{MgR}_2$ complexes for a given Lewis base, B, with a variation of the six Lewis acids ($\text{R} = \text{H}, \text{F}$ and CH_3) show much weaker correlation and are less informative. Oliveira, Kraka and Cremer [14,26] have published plots which show the variation of relative bond strength order versus local stretching force constant as a gentle, smooth curve for many halogen- and chalcogen-bonded complexes.

2.3. Nucleophilicities of B and Electrophilicities of BeR_2 and MgR_2 ($\text{R} = \text{F}, \text{H}$ or CH_3)

It has been shown that for complexes involving hydrogen bonds, halogen bonds, tetrel bonds, pnictogen bonds and chalcogen bonds, D_e can be represented by an equation of the type

$$D_e = cN_{\text{B}}E_{\text{A}} + d \quad (1)$$

where N_{B} is the nucleophilicity of the Lewis base, B, E_{A} is the electrophilicity of the Lewis acid, A, and c and d are constants. It is convenient to define $c = 1.00 \text{ kJ} \cdot \text{mol}^{-1}$ so that N_{B} and E_{A} are dimensionless. Given the direct proportionality of D_e and k_σ , Equation (1) can be recast with k_σ as the subject and indeed it was with that version of the expression that N_{B} and E_{A} were first proposed for hydrogen-bonded complexes [27]. Here, we will use the version defined as Equation (1). It has also been established that the constant term, d , is usually small and can be negligible. Whether or not that is the case, the plots of D_e versus N_{B} are usually good straight lines and it follows then that the gradient is $dD_e/dN_{\text{B}} = cE_{\text{A}}$. In the earlier determinations of N_{B} and E_{A} for the $\text{B} \cdots \text{HX}$ complexes ($\text{X} = \text{F}, \text{Cl}, \text{Br}$, etc.), the following procedure was used. The values of N_{B} were assigned to the various Lewis bases so that the plot of D_e (or k_σ) versus N_{B} for the $\text{B} \cdots \text{HF}$ complexes is a straight line through the origin. The sets of D_e for the $\text{B} \cdots \text{HCl}$, $\text{B} \cdots \text{HBr}$, etc., complexes were then plotted against N_{B} values so defined to give good straight lines, the gradients of which then defined the electrophilicities of the various HX molecules. An alternative procedure, used in [20], is to assign N_{B} and E_{A} values by a global fit of the D_e values of 250 complexes held together by a wide range of non-covalent bonds. The graphical approach, however, is useful for illustrating systematic relationships between different series of complexes and is employed here for the six BeR_2 and MgR_2 series ($\text{R} = \text{F}, \text{H}$ or CH_3).

Figure 8 shows the plots of D_e versus N_{B} for the series of $\text{B} \cdots \text{MgF}_2$, $\text{B} \cdots \text{MgH}_2$ and $\text{B} \cdots \text{Mg}(\text{CH}_3)_2$ complexes when $\text{B} = \text{CO}, \text{HCN}, \text{H}_2\text{O}, \text{NH}_3, \text{H}_2\text{S}$ or PH_3 . The values of N_{B} are those appropriate to the $\text{B} \cdots \text{HF}$ series when N_{NH_3} is set to 7.5 to be consistent with its value reported in [20]. The remainder of N_{B} are those chosen so that the points in a plot of D_e versus N_{B} for all the $\text{B} \cdots \text{HF}$ complexes (data from [20]) lie on a straight line through the origin and are given in Table 3. This line for the $\text{B} \cdots \text{HF}$ is included in Figure 8 together with plots of D_e versus N_{B} for $\text{B} \cdots \text{HCl}$ and $\text{B} \cdots \text{HBr}$ (D_e values from [20]) against the set of N_{B} defined by $\text{B} \cdots \text{HF}$. The straight lines for the $\text{B} \cdots \text{MgR}_2$ complexes are from least squares fits of the points (but with the points for $\text{B} = \text{H}_2\text{O}$ excluded for reasons given below) for each series and the gradients of the fits $dD_e/dN_{\text{B}} = cE_{\text{A}}$ lead to the E_{A} values for $\text{A} = \text{MgF}_2, \text{MgH}_2, \text{Mg}(\text{CH}_3)_2, \text{HF}, \text{HBr}$ and HCl listed in Table 3. The corresponding diagram for the $\text{B} \cdots \text{BeR}_2$ series is in Figure 10, in which the plots for $\text{B} \cdots \text{HX}$ ($\text{X} = \text{F}, \text{Cl}$ and Br) are included. The points for $\text{H}_2\text{O} \cdots \text{BeR}_2$ were again excluded from the linear regression fits. The values of E_{A} derived from the gradients are in Table 3. The N_{B} and E_{A} values determined from the global fit of the D_e values of 250 hydrogen-, halogen-, tetrel-, pnictogen- and chalcogen-bonded complexes [20] are included in Table 3 for comparison. It is clear that there is reasonably good agreement between the N_{B} values obtained here and those in ref. [20]. The same good agreement holds for the E_{A} values of HCl and HBr .

The reason for excluding the D_e values of the $\text{H}_2\text{O}\cdots\text{MgR}_2$ and $\text{H}_2\text{O}\cdots\text{BeR}_2$ complexes from Figures 8 and 10, respectively, is that they imply $N_{\text{H}_2\text{O}}$ values which significantly exceed those obtained from the $\text{B}\cdots\text{HF}$ data here (5.24) or from the global fit (4.89) in ref. [20] for H_2O . If the value of D_e for each $\text{H}_2\text{O}\cdots\text{MgR}_2$ were forced to lie on its appropriate regression line in Figure 8, the value $N_{\text{H}_2\text{O}} \approx 6.4$ would be necessary for each R. A similar conclusion applies for the $\text{B}\cdots\text{BeR}_2$ complexes, implying that $N_{\text{H}_2\text{O}} \approx 6.1$. Thus, H_2O has a higher electrophilicity for the MR_2 molecules than it does for HF . This could be related to the efficacy of water as a solvent for ions.

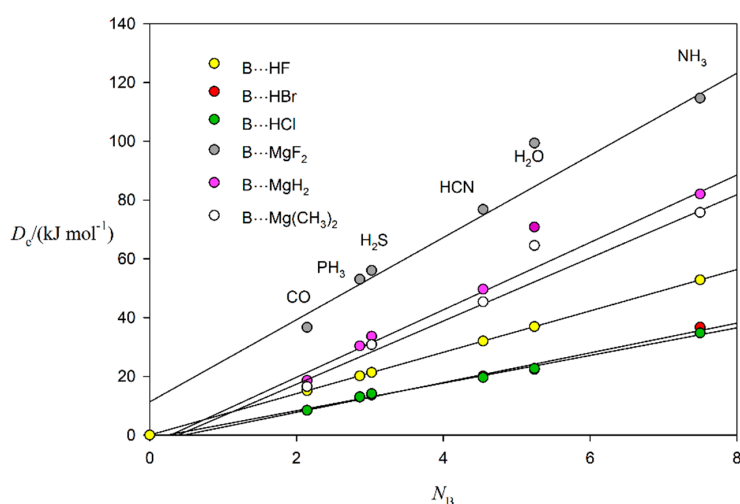


Figure 8. D_e versus the nucleophilicity, N_B , for the $\text{B}\cdots\text{MgR}_2$ series and $\text{B}\cdots\text{HX}$ complexes ($\text{B} = \text{CO}$, HCN , H_2O , NH_3 , H_2S and PH_3 ; $\text{R} = \text{F}$, H or CH_3 ; $\text{X} = \text{F}$, Cl or Br). The N_B values are defined by the $\text{B}\cdots\text{HF}$ straight line through the origin (see text for details). The points for $\text{H}_2\text{O}\cdots\text{MgR}_2$ were excluded from the regression fits for reasons discussed in the text. The lines and points for $\text{B}\cdots\text{HCl}$ and $\text{B}\cdots\text{HBr}$ are almost coincident. ($R^2 = 0.994, 0.994, 0.990, 1.000, 0.993$ and 0.988 for the $\text{Mg}(\text{CH}_3)_2$, MgH_2 , MgF_2 , HF , HCl and HBr lines, respectively).

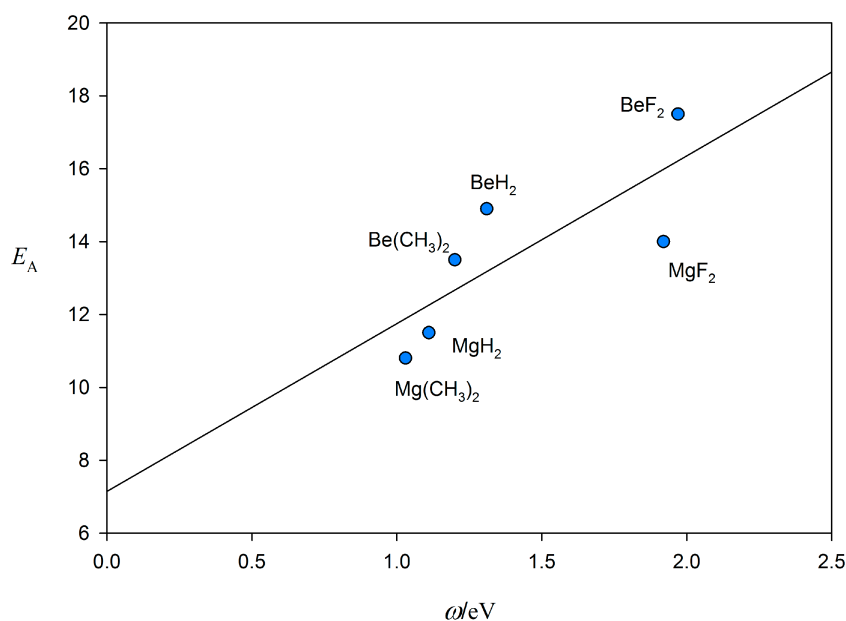


Figure 9. The relationship between the conceptual DFT electrophilicity index, ω , calculated from Equation (2) at the CCSD/aug-cc-pVTZ//CCSD(T)/aug-cc-pVTZ level of theory, and the E_A determined here for various MR_2 molecules ($\text{M} = \text{Be}$ or Mg , $\text{R} = \text{F}$, H , or CH_3).

Table 3. Nucleophilicities of six Lewis bases, B, and electrophilicities of nine Lewis acids, A.

Lewis Base B	Nucleophilicities		Lewis Acid A	Electrophilicities	
	N_B (This Work) ^a	N_B (From [20]) ^b		E_A (This Work) ^c	E_A (From [20]) ^b
CO	2.14	2.12	BeF ₂	17.5(4)	-
PH ₃	2.86	3.12	BeH ₂	14.9(6)	-
H ₂ S	3.02	3.43	Be(CH ₃) ₂	13.5(6)	-
HCN	4.54	4.27	MgF ₂	14.0(8)	-
H ₂ O	5.24	4.89	MgH ₂	11.5(5)	-
NH ₃	7.50	7.52	Mg(CH ₃) ₂	10.8(6)	-
			HF	7.0	6.75
			HBr	5.1(3)	4.59
			HCl	4.7(2)	4.36

^a Calculated by assuming that $D_e = cN_B E_A$ with $c = 1.00 \text{ kJ} \cdot \text{mol}^{-1}$ and $N_{\text{NH}_3} = 7.50$ and that all D_e for the B...HF complexes (from ref. [21]) lie on a straight line through the origin. ^b Values from ref. [20] when determined by a global fit to D_e values of 250 complexes held together by various types of non-covalent bonds. ^c Obtained from the gradient $dD_e/dN_B = cE_A$ of the linear regression fit of each set of points in Figures 9 and 10.

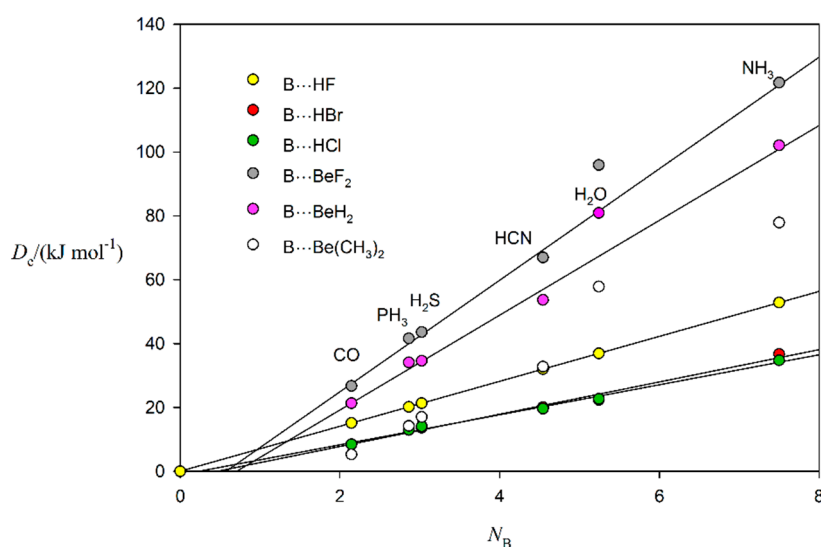


Figure 10. D_e versus the nucleophilicity, N_B , for the series B...BeR₂ and B...HX complexes (B = CO, HCN, H₂O, NH₃, H₂S and PH₃; R = F, H or CH₃; X = F, Cl or Br). The N_B values are defined by the B...HF straight line through the origin (see text for details). The points for H₂O...BeR₂ were excluded from the regression fits for reasons discussed in the text. The regression lines and points for B...HCl and B...HBr are almost coincident. To avoid congestion, the regression line for the B...Be(CH₃)₂ points has been omitted. ($R^2 = 0.994, 0.996, 0.998, 1.000, 0.993$ and 0.988 for Be(CH₃)₂, BeH₂, BeF₂, HF, HCl and HBr lines, respectively).

It is possible to estimate a value of the electrophilicity index, ω , as defined by the conceptual DFT method [28]. This index is given in terms of the energies of the lowest energy-unoccupied and the highest energy-occupied molecular orbitals (E_{LUMO} and E_{HOMO}), respectively, by the expression

$$\omega \approx (E_{\text{HOMO}} + E_{\text{LUMO}})^2 / 8(E_{\text{LUMO}} - E_{\text{HOMO}}) \quad (2)$$

When E_{LUMO} and E_{HOMO} are calculated at the CCSD/aug-cc-pVTZ//CCSD(T)/aug-cc-pVTZ level of theory, the results for ω are 1.97, 1.31 and 1.20 eV for BeF₂, BeH₂ and Be(CH₃)₂, respectively, and 1.92, 1.11 and 1.03 eV for MgF₂, MgH₂ and Mg(CH₃)₂, respectively. Figure 9 shows a plot of the E_A values from the present work against ω . There is a reasonable correlation between the two measures of the electrophilicity of the six MR₂.

3. Theoretical Methods

The equilibrium geometries, dissociation energies, D_e , and force constants, k_σ , were obtained at the CCSD(T) computational level [29] for each $B\cdots BeR_2$ and $B\cdots MgR_2$ complex investigated. In the first step of the calculations, the geometry of the monomers and complexes was optimized with the aug-cc-pVTZ basis set [30] at the CCSD(T) level. A geometry scan of the intermolecular distance of ± 0.1 Å from the optimized value, r_e , was then determined in steps of $(r - r_e) = 0.025$ Å at the same computational level to yield the variation of the energy $E(r - r_e)$ with the displacement $(r - r_e)$ from equilibrium. As an example, the resulting curve for the $OC\cdots BeF_2$ complex is given in Figure 11. Such curves were then fitted by a third-order polynomial in $(r - r_e)$, from which k_σ is obtained as the numerical value of the second derivative of E with respect to $(r - r_e)$ evaluated at r_e . In order to obtain more accurate D_e values, complete basis set (CBS) extrapolation [CCSD(T)/CBS energy] was executed by using the CCSD(T)/aug-cc-pVTZ//CCSD(T)/aug-cc-pVTZ and CCSD(T)/aug-cc-pVQZ//CCSD(T)/aug-cc-pVTZ energies for all the systems [31,32]. Thus, the D_e values have been obtained as the difference of the CCSD(T)/CBS energy of the monomers and the complex. All ab initio calculations were performed with the MOLPRO-2012 program [33]. The molecular electrostatic potential surfaces of the various BeR_2 and MgR_2 monomers were calculated on the 0.001 e/bohr³ electron density isosurface at the CCSD/aug-cc-pVTZ//CCSD(T)/aug-cc-pVTZ level of theory by using the Gaussian-16 Program [24]. Tables 1 and 2 include the D_e and k_σ values for all complexes investigated here.

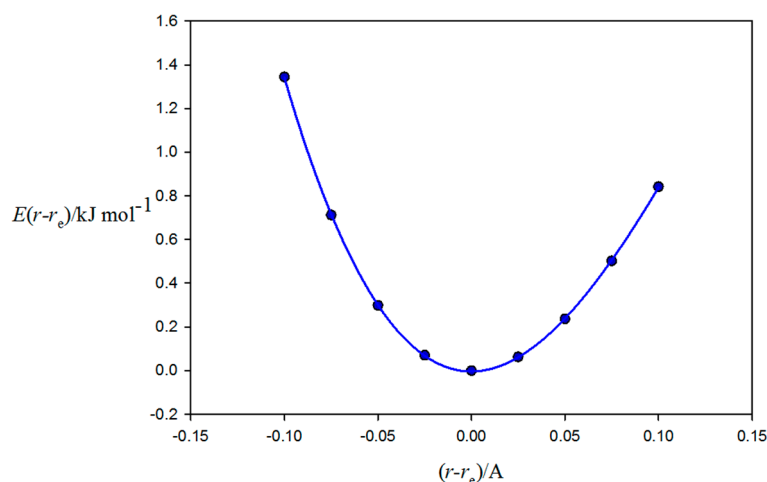


Figure 11. Variation of the energy $E(r - r_e)$ of $OC\cdots BeF_2$ as a function of the displacement $(r - r_e)$ from the global minimum at r_e along the C_2 axis of this Y-shaped complex. (F–Be–F) forms the arms of the Y and CO forms the stem. See Figure 3 for a molecular diagram. The geometry was re-optimized at each of the indicated points and the line through the points is the third-order polynomial curve from the regression fit to the points. The second derivative evaluated at r_e gives the intermolecular stretching force constant, k_σ . The corresponding curves and the fitted polynomials for all $B\cdots BeR_2$ and $B\cdots MgR_2$ complexes ($B = CO, H_2S, PH_3, HCN, H_2O$ or NH_3 ; $R = F, H$ or CH_3) investigated here are available in the Supplementary Material.

4. Conclusions

Ab initio calculations at the CCSD(T)/aug-cc-pVTZ level have yielded the geometries, intermolecular stretching force constants, k_σ , and dissociation energies, D_e , of the 18 $B\cdots BeR_2$ complexes ($B = CO, HCN, H_2O, NH_3, H_2S$ or PH_3 and $R = F, H$ or CH_3) and of the corresponding set of complexes in which Be is replaced by Mg. In all cases, D_e was determined by using the complete basis set extrapolation. The dissociation energies, D_e , reveal that, for a given R, the complexes involving Mg are more strongly bound than those involving Be—a conclusion that is consistent with the greater maximum positive MEPS for the former (see Figure 1 and Figure S1 of Supplementary

Material). It has been shown that all the complexes have a Y shape that can be understood as follows. The free MR_2 molecules are linear (see Figure 2). The following process may then be envisaged. The Lewis base, B, is assumed to approach MR_2 so that the non-bonding electron pair of B (the most nucleophilic region of B) interacts with the belt of high electrophilicity that lies around the M atom (see blue regions in Figure 1) to give an initially T-shaped complex. As the Lewis base becomes closer, the linear R-M-R subunit distorts, with the R atoms/groups moving away from B to give the Y shape. One might envisage the following electronic description of the process. The two valence-shell electrons of the metal atom, M, in MR_2 are assumed to singly occupy sp_z hybrids, which then form single bonds with F or H or C to give the linear molecules F-M-F, H-M-H and $\text{H}_3\text{C-M-CH}_3$, respectively. The electrophilic (relatively positive) belt around the metal atom, M, and perpendicular to the F-M-F line, is presumably a consequence of the empty np_x and np_y orbitals ($n=2$ for $\text{M} = \text{Be}$ and $n=3$ for $\text{M} = \text{Mg}$). As the non-bonding pair of B approaches and interacts with an empty p_x or p_y orbital, the hybridization at M changes gradually to take on some sp^m character. As m increases from 1 to 2, the angular deviation, θ (see Figure 3 for the definition of θ) from linearity, should increase from 0° to 30° , the latter corresponding to an R-M-R angle of 120° . We note from Tables 1 and 2 that for a given M and R, the angle, θ , tends to increase as the binding strength (D_e or k_σ) increases and about 20° for the most strongly bound complexes, namely, those involving H_2O and NH_3 with BeR_2 . Moreover, the lengthening $\delta r(\text{M-R})$ of the M-R bond tends to increase with binding strength. Both observations are consistent with a change from sp towards sp^2 hybridization. Thus, it appears that the interaction of B and MR_2 can be described as partly electrostatic and partly dative in character. It is noted that the dative bond character appears greater when $\text{M} = \text{Be}$ than when $\text{M} = \text{Mg}$, with the non-linearities θ closer to 30° , with larger values of $\delta r(\text{M-R})$ and presumably values of m closer to 2 in the sp^m hybridization scheme. It appears, therefore, that these are not purely σ -hole/ n -pair interactions.

The shapes of the $\text{B}\cdots\text{BeR}_2$ and $\text{B}\cdots\text{MgR}_2$ complexes can be predicted by a simple modification to a rule recently enunciated [20] for tetrel-bonded complexes of the type $\text{B}\cdots\text{CO}_2$, that is:

The equilibrium geometry of alkaline-earth bonded $\text{B}\cdots\text{MR}_2$ complexes ($\text{M} = \text{Be}, \text{Mg} \dots$) can be predicted by assuming that a radius of the most electrophilic ring around the M atom that is perpendicular to the MR_2 line coincides with the axis of a non-bonding electron pair carried by B. Some deviation of MR_2 from collinearity could occur.

For both sets of $\text{B}\cdots\text{BeR}_2$ and $\text{B}\cdots\text{MgR}_2$ complexes, it has been established that D_e is directly proportional to k_σ to a good degree of approximation, as seen from Figures 6 and 7. Moreover, as with more weakly bound complexes such as $\text{B}\cdots\text{HX}$ ($\text{X} = \text{F}, \text{Cl}, \text{Br}$), it has been possible to partition D_e into contributions from the individual molecules B and MR_2 , called the nucleophilicity, N_B , of the Lewis base, B, and the electrophilicity, E_A , of the Lewis acid, A, respectively. As may be seen from Table 3, the order of the E_A values for both BeR_2 and MgR_2 sets when acting as Lewis acids is $\text{R} = \text{F} > \text{H} \geq \text{CH}_3$, which is the order expected from the $-I$ inductive effect of F relative to H and the $+I$ effect of the CH_3 group relative to H, and is the order indicated by the MEPS in Figure 1. The $-I$ effect of F is evidently greater than the $+I$ effect of CH_3 . It is also clear from Table 3 that for a given R, the electrophilicity of BeR_2 is greater than that of MgR_2 . This appears to be at variance with the MEPS, because the electrophilic (blue) belt around M is more positive for $\text{M} = \text{Mg}$ than Be, with, for example, the maximum positive potentials for MgF_2 and BeF_2 at 753 and 337 kJ mol^{-1} , respectively (see Figure 1 and Introduction). It is of interest that the order of electrophilicities given in Table 3 is $\text{BeF}_2 > \text{BeH}_2 > \text{Be}(\text{CH}_3)_2 \sim \text{MgF}_2 > \text{MgH}_2 > \text{Mg}(\text{CH}_3)_2 \gg \text{HF} > \text{HBr} \sim \text{HCl}$, which indicates just how effective BeR_2 and MgR_2 are as Lewis acids. Various other scales of nucleophilicity and electrophilicity have been proposed. Some are based on the rate constants for organic reactions in solution [34], while others have been based on conceptual density functional theory (CDFT) [28]. A comparison of our results for the E_A of MR_2 with those estimated by the CDFT approach has been presented.

We have shown that the BeR_2 and MgR_2 Lewis acids discussed here undergo non-covalent interactions with a series of Lewis bases, all of which can provide a non-bonding electron pair to interact with the electrophilic belt that encircles the central metal atom in MR_2 . Evidently, these interactions

can be described as beryllium bonds and magnesium bonds, respectively, by analogy with the recent definitions [6,7,18] of other non-covalent interactions such as halogen-, tetrel-, pnictogen-, chalcogen- and coinage-metal bonds. Therefore, we propose the following definition:

A alkaline-earth non-covalent bond occurs when there is evidence of a net attractive interaction between an electrophilic region associated with an atom of an element, E{II}, in a molecular entity and a nucleophilic region (e.g., a n-pair or π -pair of electrons) in another, or the same, molecular entity, where E{II} is an element of Group II in the periodic table.

Note that this definition is coherent with the IUPAC definition of the halogen bond [7].

Supplementary Materials: The following are available online at <http://www.mdpi.com/2304-6740/7/3/35/s1>, Figure S1: Molecular electrostatic surface potentials of the linear, non-polar molecules, MgF_2 , MgH_2 and $\text{Mg}(\text{CH}_3)_2$ calculated at the 0.001 e/bohr³ electron density isosurface at the CCSD/aug-cc-pVTZ//CCSD(T)/aug-cc-pVTZ level of theory, Table S1: Optimized geometry, electronic energy and Variation of the energy $E(r-r_e)$ as a function of the displacement ($r-r_e$) from the global minimum at r_e at the CCSD(T)/aug-cc-pVTZ computational level.

Author Contributions: The conceptualization of the project, the calculations, the writing of the manuscript, the drawing of figures, checking of proofs, etc. were shared between I.A. and A.C.L.

Funding: This research was funded by Consejería de Educación e Investigación de la Comunidad de Madrid (P2018/EMT-4329 AIRTEC-CM) and Ministerio de Ciencia, Innovación y Universidades (PGC2018-094644-B-C22).

Acknowledgments: I.A. thanks Consejería de Educación e Investigación de la Comunidad de Madrid (P2018/EMT-4329 AIRTEC-CM) and Ministerio de Ciencia, Innovación y Universidades (PGC2018-094644-B-C22). A.C.L. thanks the University of Bristol for a Senior Research Fellowship.

Conflicts of Interest: The authors declare no conflict of interest.

References

- Hassel, O.; Rømming, C. Direct structural evidence for weak charge-transfer bonds in solids containing chemically saturated molecules. *Quart. Rev. Chem. Soc.* **1962**, *16*, 1–18. [CrossRef]
- Ligon, A.C. Pre-reactive complexes of dihalogens XY with Lewis bases B in the gas phase: A systematic case for the ‘halogen’ analogue $B \cdots XY$ of the hydrogen bond $B \cdots HX$. *Angew. Chem. Int. Ed. Engl.* **1999**, *38*, 2686–2714. [CrossRef]
- Neukirch, H.; Pilati, T.; Resnati, G. Halogen bonding based recognition processes: World parallel to hydrogen bonding. *Acc. Chem. Res.* **2005**, *38*, 386–395.
- Metrangolo, P.; Resnati, G. (Eds.) Halogen bonding 1, Impact on Materials and Life Sciences. In *Topics in Current Chemistry*; Springer: Berlin, Germany, 2015; Volume 358, pp. 1–280.
- Ligon, A.C. The halogen bond: An interim perspective. *Phys. Chem. Chem. Phys.* **2010**, *12*, 7736–7747. [CrossRef] [PubMed]
- Arunan, E.; Desiraju, G.R.; Klein, R.A.; Sadlej, J.; Scheiner, S.; Alkorta, I.; Clary, D.C.; Crabtree, R.H.; Dannenberg, J.J.; Hobza, P.; et al. Definition of the hydrogen bond (IUPAC Recommendations 2011). *Pure Appl. Chem.* **2011**, *83*, 1637–1641. [CrossRef]
- Desiraju, G.R.; Ho, P.S.; Kloo, L.; Ligon, A.C.; Marquardt, R.; Metrangolo, P.; Politzer, P.A.; Resnati, G.; Rissanen, K. Definition of the halogen bond (IUPAC Recommendations 2013). *Pure Appl. Chem.* **2013**, *85*, 1711–1713. [CrossRef]
- Ligon, A.C. Tetrel, pnictogen and chalcogen bonds identified in the gas phase before they had names: A systematic look at non-covalent interactions. *Phys. Chem. Chem. Phys.* **2017**, *19*, 14884–14896. [CrossRef] [PubMed]
- Alcock, N.W. Secondary bonding to non-metallic elements. *Adv. Inorg. Chem. Radiochem.* **1972**, *15*, 1–58.
- Bauzá, A.; Mooibroek, T.J.; Frontera, A. Tetrel-bonding interaction: Rediscovered supramolecular force? *Angew. Chem. Int. Ed.* **2013**, *52*, 12317–12321. [CrossRef] [PubMed]
- Zahn, S.; Frank, R.; Hey-Hawkins, E.; Kirchner, B. Pnictogen bonds: A new molecular linker? *Chem. Eur. J.* **2011**, *17*, 6034–6038. [CrossRef] [PubMed]
- Wang, W.; Ji, B.; Zhang, Y. Chalcogen bond: A sister noncovalent bond to halogen bond. *J. Phys. Chem. A* **2009**, *113*, 8132–8135. [CrossRef] [PubMed]

13. Categorizing Chalcogen, Pnictogen, and Tetrel Bonds, and Other Interactions Involving Groups 14–16 Elements. Available online: https://iupac.org/projects/project-details/?project_nr=2016-001-2-300 (accessed on 15 January 2019).
14. Oliveira, V.; Cremer, D.; Kraka, E. The many facets of chalcogen bonding described by vibrational spectroscopy. *J. Phys. Chem.* **2017**, *121*, 6845–6862. [CrossRef] [PubMed]
15. Varadwaj, P.R.; Varadwaj, A.; Marques, H.M.; Yamashita, K. Can combined electrostatics and polarization effects alone explain the F...F negative-negative bonding in simple fluoro-substituted benzene derivatives. *Computation* **2018**, *6*, 51. [CrossRef]
16. Wang, C.W.; Fu, Y.Z.; Zhang, L.N.; Danovich, D.; Shaik, S.; Mo, Y. Hydrogen and halogen bonds between ions of like charges: Are they anti-electrostatic in nature? *J. Comput. Chem.* **2018**, *39*, 481–487. [CrossRef] [PubMed]
17. Clark, T. Hydrogen bonds and σ holes. *Faraday Discuss.* **2017**, *203*, 9–27. [CrossRef] [PubMed]
18. Legon, A.C.; Walker, N.R. What's in a name? "Coinage-metal" non-covalent bonds and their definition. *Phys. Chem. Chem. Phys.* **2018**, *20*, 19332–19338. [CrossRef] [PubMed]
19. Yáñez, M.; Sanz, P.; Mó, O.; Alkorta, I. and Elguero, J. Beryllium bonds, do they exist? *J. Chem. Theory Comput.* **2009**, *5*, 2763–2771. [CrossRef] [PubMed]
20. Alkorta, I.; Legon, A.C. Nucleophilicities of Lewis bases B and electrophilicities of Lewis acids A determined from the dissociation energies of complexes B...A involving hydrogen bonds, tetrel bonds, pnictogen bonds, chalcogen bonds and halogen bonds. *Molecules* **2017**, *22*, 1786. [CrossRef] [PubMed]
21. Alkorta, I.; Legon, A.C. Strengths of non-covalent interactions in hydrogen-bonded complexes B...HX and halogen-bonded complexes B...XY (X, Y = F, Cl): An ab initio investigation. *New J. Chem.* **2018**, *42*, 10548–10554. [CrossRef]
22. Legon, A.C. A reduced radial potential energy function for the halogen bond and the hydrogen bond in complexes B...XY and B...HX, where X and Y are halogen atoms. *Phys. Chem. Chem. Phys.* **2014**, *16*, 12415–12421. [CrossRef] [PubMed]
23. Ingold, C.K. *Structure and Mechanism in Organic Chemistry*; Cornell University Press: Ithaca, NY, USA, 1953; Chapter 2; pp. 67–72.
24. Frisch, M.J.; Trucks, G.W.; Schlegel, H.B.; Scuseria, G.E.; Robb, M.A.; Cheeseman, J.R.; Scalmani, G.; Barone, V.; Petersson, G.A.; Nakatsuji, H.; et al. *Gaussian 16*; Revision B.01; Gaussian, Inc.: Wallingford, CT, USA, 2016.
25. Anusiewicz, I.; Skurski, P. An ab initio study on BeX₃[−] superhalogen anions (X = F, Cl, Br). *Chem. Phys. Lett.* **2002**, *358*, 426–434. [CrossRef]
26. Oliveira, V.; Kraka, E.; Cremer, D. Quantitative assessment of halogen bonding utilizing vibrational spectroscopy. *Inorg. Chem.* **2017**, *56*, 488–502. [CrossRef] [PubMed]
27. Legon, A.C.; Millen, D.J. Hydrogen bonding as a probe for electron densities: Limiting gas phase nucleophilicities and electrophilicities of B and HX. *J. Am. Chem. Soc.* **1987**, *109*, 356–358. [CrossRef]
28. Domingo, L.R.; Rios-Gutiérrez, M.; Pérez, P. Applications of the conceptual density functional theory indices to organic chemistry reactivity. *Molecules* **2016**, *21*, 748. [CrossRef] [PubMed]
29. Purvis, G.D., III; Bartlett, R.J. A full coupled-cluster singles and doubles model—The inclusion of disconnected triples. *J. Chem. Phys.* **1982**, *76*, 1910–1918. [CrossRef]
30. Dunning, T.H., Jr. Gaussian basis sets for use in correlated molecular calculations. I. The atoms boron through neon and hydrogen. *J. Chem. Phys.* **1989**, *90*, 1007–1023. [CrossRef]
31. Feller, D. The use of systematic sequences of wave functions for estimating the complete basis set, full configuration interaction limit in water. *J. Chem. Phys.* **1993**, *98*, 7059–7071. [CrossRef]
32. Halkier, A.; Helgaker, T.; Jorgensen, P.; Klopper, W.; Olsen, J. Basis-set convergence of the energy in molecular Hartree–Fock calculations. *Chem. Phys. Lett.* **1999**, *302*, 437–446. [CrossRef]
33. Werner, H.-J.; Knowles, P.J.; Knizia, G.; Manby, F.R.; Schütz, M.; Celani, P.; Korona, T.; Lindh, R.; Mitrushenkov, A.; Rauhut, G.; et al. MOLPRO, Version 2012.1. Available online: <http://www.molpro.net> (accessed on 15 January 2019).
34. Mayr, H.; Patz, M. Scales of nucleophilicity and electrophilicity: A system of ordering polar organic and organometallic reactions. *Angew. Chem. Int. Ed. Engl.* **1994**, *33*, 938–957. [CrossRef]

